29th Congress of the International Council of the Aeronautical Sciences
St. Petersburg, Russia; September 7-12, 2014

LAMINAR-TURBULENT TRANSITION CONTROL BY DIELECTRIC BARRIER DISCHARGE. THEORY AND EXPERIMENT

M.V. Ustinov*, A.A. Uspensky*, A. Yu. Urusov*, D.A. Rusianov*
***Central Aerohydrodynamic Institute (TsAGI)**

Keywords: *barrier discharge, laminar-turbulent transition*

Abstract

Recent results of investigations of laminar-turbulent transition control by dielectric barrier discharge (DBD) in TsAGI are presented. Delay of natural transition in the flat-plate boundary layer by means of flow acceleration by discharge on one or three normal to flow direction electrodes was studied experimentally in quiet wind tunnel. Optimal electrodes locations and regime of discharge provided maximal downstream shift of transition were found. Phenomenological model of force induced by DBD actuator was developed and verified experimentally. This model was applied to numerical modeling of cross-flow dominated transition control by multi-electrode DBD actuator.

1 Introduction

Flow control by means of dielectric barrier discharge actuators is studied extensively last ten years. Physics of this type of electric discharge and gas flow induced by it was investigated in [1]. Its action on the gas flow can be modeled by combination of steady body force and heat release [2,3]. Usually DBD actuators were used for airfoil lift enhancement by means of stall prevention [4]. However, such lift control is suitable for low speed only because of weak flow velocity (<10m/sec) induced by DBD. DBD application to boundary layer laminarization seems to be more attractive because of minimal change of velocity profile can improve boundary layer stability. Computations [3] showed that 2-3% increase of near-wall flow velocity leads to two-fold increase of laminar flow region. High efficiency of cross-flow dominated transition control by DBD for transonic speed was demonstrated in theoretical work [5]. In experiments [3,6] reduction of growth rates of artificially introduced growth rates and transition delay using DBD was obtained. In [6] demonstrated the possibility of TS wave cancellation by means of generation of artificial disturbances of opposite phase by DBD modulated by low-frequency signal was demonstrated. Discharge-induced streamwise vortices were used in [7] for by-pass transition control.

All previously mentioned experiments deal with transition caused by artificially introduced disturbances of relatively large amplitude. However, possibility of natural transition delay by DBD is not clear for discharge may become the main source of unstable disturbances in this case. The present work deals with experimental study of natural transition delay by DBD in low-turbulence wind tunnel. Another purpose of work is development and testing of numerical methods for computation of discharge influence on swept-wing boundary layer and laminar-turbulent transition caused by cross-flow instability.

2. Experimental study of laminar-turbulent transition delay by dielectric barrier discharge

2.1 Experimental setup & conditions

Experiment was performed in the low-turbulence direct flow wind tunnel T36I of TsAGI. Its test section is 2.6 *m* long, 0.5 *m* wide and 0.35 *m* high, and is preceded by a 12:1 contraction. The free-stream turbulence level in

the test section is 0.06% measured in the band 5-1500Hz. Measurements were made in the boundary layer on the floor of test section for flow velocity 8-15 *m/s*. Plasma actuator with three normal to flow direction electrodes was placed in the hatch located at the distance of 1100 mm from the beginning of the test section. Dielectric barrier discharge at any pair of electrodes may be turned on or off. It was powered by high-voltage-impulses generator which initiates rectangular impulses of duration $\tau = 20\mu s$. Four regimes of generator operation were used in experiment. Amplitude of impulses V and its frequency f for these regimes are listed in Table 1. Outline of experimental facility and design of plasma actuator are shown in Fig. 1.

Table 1. Parameters of generator operation regimes

regime	f,kHz	V,kV
1	6.25	4.4
2	3.12	4.4
3	12.5	4.4
4	12.5	3.3

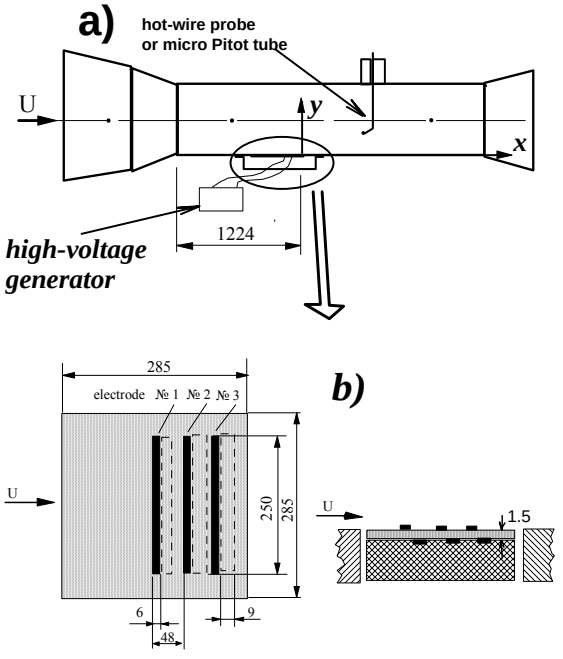

Fig 1. Experimental set-up (a), and plasma actuator design (b). Dimensions are in millimeters

Averaged value and pulsations of streamwise velocity in the boundary layer were measured by constant temperature hot-wire anemometer. All measurements were made in the vertical plane in the middle of the test section. Coordinate system with origin on the trailing edge of the third electrode and *x, y* axes directed along the flow and vertically will be used for description of the results.

2.2 Boundary layer and laminar-turbulent transition without discharge

At first the state of boundary layer on the floor of test section without discharge was investigated. Main boundary layer characteristics as functions of streamwise coordinate are shown in Fig 2. Outer flow velocity distribution measured in the mid-high of the test section (*y=175* mm) reveals slight adverse pressure gradient with velocity drops approximately to 1% over 1 meter. R.m.s. velocity pulsations measured for different flow velocity reveals that transition moves upstream with increase of speed. This fact indirectly justifies that transition to turbulence on the floor of the test section is really natural. Most of subsequent results were obtained for flow velocity 10 m/s and this value of velocity will be assumed on default if another is not declared. For this value of flow velocity transition found from the maximum of pulsations is located at *x=400* mm.

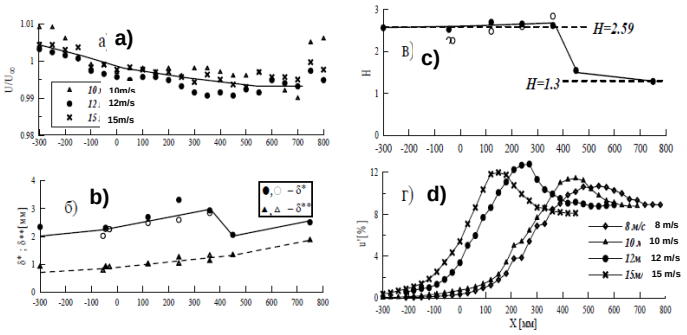

Fig 2. Parameters of boundary layer on the floor of the test section without discharge. (a) – outer flow velocity, (b) – displacement and momentum loss thicknesses, (c) – shape factor H= δ^* / δ^{**} , (d) – velocity pulsations.

In the laminar part the boundary layer is well described by the Blasius solution with virtual leading edge location x=-1490mm. Its shape factor here is close to theoretical value for Blasius velocity profile H=2.59. Near the

transition point it drops to characteristic value H=1.3 for turbulent boundary layer. Transition Reynolds number estimated from displacement thickness is $R_{\delta*} \approx 2000$ and corresponds to Reynolds number $R_x = 1.3 \times 10^6$ based on the length of equivalent plate. Such earlier transition could not be caused by weak adverse pressure gradient and is probably initiated by disturbances coming from transitional boundary layer on the side walls of the test section.

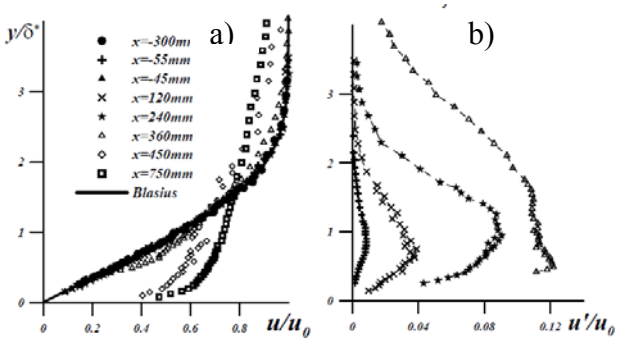

Fig 3. Profiles of velocity (a) and its r.m.s. pulsations (b) in the boundary layer without discharge for $u_\infty = 10 m/s$

Profiles of mean velocity and pulsations in boundary layer are presented in Fig. 3. Velocity profiles measured before the transition fall on Blasius profile. Maxima of pulsations here are located at distance $0.7\delta*$ from the wall which is familiar for maximal pulsations in Tollmien-Schlichting wave. Last velocity profile measured at *x=750* mm is fully turbulent.

2.3 Effect of DBD on laminar-turbulent transition

Influence of regime of generator operation on the transition location was investigated initially. Results obtained in form of amplification curves of velocity pulsations for different discharge regimes are presented in Fig 4. It shows that transition is rather sensitive to the discharge parameters. Maximal downstream shift of transition ~150mm was obtained for regime #1. Regime #2 with two-fold lower frequency delays transition also, but the shift of transition point is two times smaller. High-frequency regimes of discharge #3 and #4 move transition upstream. These high-power regimes of discharge (the power of discharge is roughly proportional to a product of relative time of high voltage action and its amplitude) excite too large pulsations in the boundary layer near the electrode. Mechanism of these disturbances origination is not clear and they may be probably caused by inflexible instability of boundary layer velocity profile with a strong near-wall jet.

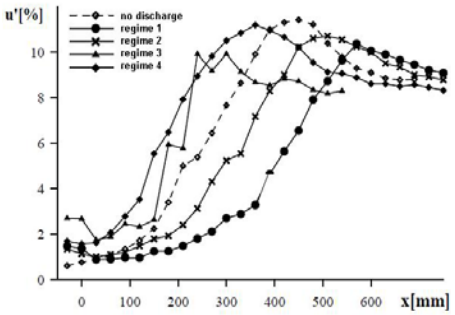

Fig 4. Influence of regime of discharge on laminar-turbulent transition for $u_\infty = 10 m/s$

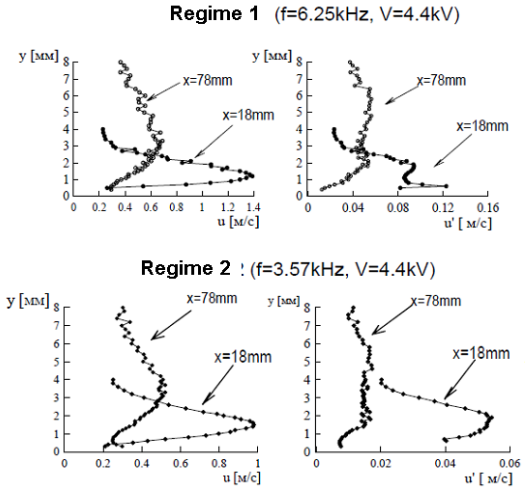

Figure 5. Flow produced by discharge in regimes #1 and 2 in a still air

Figure 5 shows flow induced by regimes #1 and #2 of discharge in a still air. Near the electrode the discharge produces a thin near-wall jet which becomes weaker and spreads as distance from electrode increases. Relatively high pulsations (of amplitude 9% and 5% from maximal velocity for regimes #1 and#2 respectively) are present in discharge-induced jet. Large amplitude of pulsations in flow induced by regime #1 of discharge permit us to conclude that this flow is a pre-transitional. Jets

induced by rather more powerful figh-frequency regimes of discharge #3 and #4 should be entirely turbulent. This may be a reason for its negative influence on laminar-turbulent transition in boundary layer.

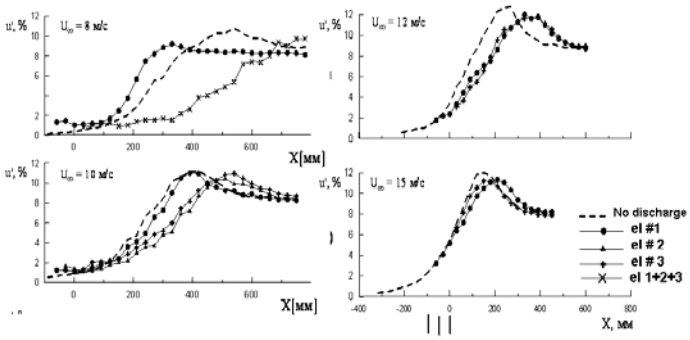

Fig. 6. Influence of discharge (regime#1) location on laminar-turbulent transition for different flow velocity

The next topic of investigation was finding of optimal discharge location which gives maximal delay of transition. This was made by means of measurements of pulsations distribution along the boundary layer for discharge in regime #1 on different electrodes. Such results obtained for flow velocities 8, 10, 12 and 15 m/s are shown in Figure 6. Its analysis results in conclusion that optimal location of discharge is the place where natural pulsations amplitude is near to 1%. This can be illustrated by two ways. The first one is consideration of amplification curves for flow velocity 10 m/s. In these conditions the best results gives the discharge on electrode #2. Discharge on electrode #1 which is too far from transition point gives only minimum transition delay. Action of discharge on the electrode #3 located closer to transition point is also some weaker then effect of discharge on electrode #2. Another way to change the position of discharge with respect to transition point is to vary flow velocity for discharge on fixed electrode. Let's consider the action on transition discharge on electrode #1 for different flow velocity. For small velocity 8 m/s, discharge on this electrode moves transition upstream. Increase of flow velocity moves transition point to discharge location and its action on transition becomes neutral for u_∞=10m/s. Further increase of velocity to 12 m/s results in transition delay by discharge on electrode 1. Its effect becomes the best (compared with action of discharge on other electrodes) for maximal flow velocity 15 m/s.

Existence of optimal discharge location may be explained as follows. When discharge is too far from transition point, discharge induced pulsations well exceed natural disturbances. So, negative effect of increase of pulsation level exceeds stabilizing effect of change of velocity profile. If the discharge is too close to transition, discharge-induced change of velocity profile can not prevent fast non-linear growth of disturbances. In optimal location discharge only slightly change the amplitude of pulsations but change of velocity profile is enough to reduce the growth rates of linearly developing perturbations.

Influence of discharge on electrode #2 on laminar-turbulent transition was studied in more details for near-optimal for this discharge location flow velocity 10m/s. Fig. 7 shows its effect on profiles of mean velocity and pulsations in the boundary layer. Acceleration of velocity in the near-wall region by discharge is well seen in two nearest to discharge sections x=-27 and 170 mm. Maximal flow acceleration by discharge is approximately equal in both sections and is estimated as 5% from outer flow velocity. Theoretically it should be enough for two-fold transition delay in accordance of results of [3].

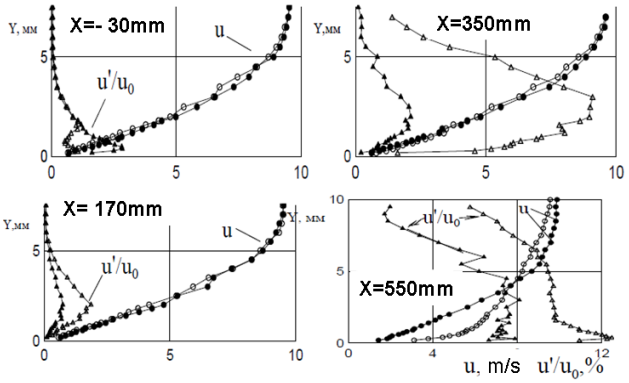

Fig. 7. Influence of discharge on profiles of mean velocity and its pulsations in the boundary layer for $u_\infty = 10 m/s$. Open and filled symbols shows results without and with discharge respectively.

Fig. 7 also illustrates the influence of discharge on development of pulsations in the boundary layer. Near the electrode discharge drastically increases the pulsations amplitude, however

discharge-induced pulsations are concentrated near the wall well below the maximum of natural disturbances. Further downstream, stabilization of the velocity profile by discharge leads to substantial reduction of pulsations. It leads to change of flow regime from turbulent to laminar in section *x=550* mm.

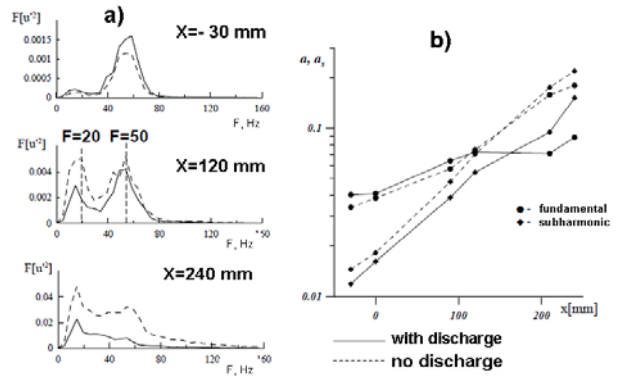

Fig 8. Influence of discharge on velocity pulsations spectra (a), and amplification rates of disturbances of fundamental and subharmonical frequency (b)

Influence of discharge on pulsations spectra shows figure 8. In the vicinity of electrode (x=-30mm) discharge increases the pulsations of fundamental frequency. Its influence on subharmonic in this section is minimal. Further downstream discharge effectively reduces the amplitude of both main TS wave and subharmonic. Growth of fundamental frequency peak in the spectrum is fully suppressed on the interval from 120 to 210mm. However, discharge action on subharmonic is not so pronounced.

3. Computational investigation of discharge influence on boundary layer flow and its stability

3.1 Problem formulation and numerical method

To understand the influence of parameters of DBD actuators on the boundary layer the computational studies of flow modification by DBD were performed. Presumptive configuration of electrodes of actuator intended for laminar-turbulent transition delay in the boundary layer at the infinite-span swept wing is shown in Fig. 9, a.

Two cartesian co-ordinate systems x_v, y_v, z fitted to wing leading edge and x, y, z fitted to the last electrode of actuator will be used for flow description. The angle between the axes x_v and x is named as electrode inclination angle ψ.

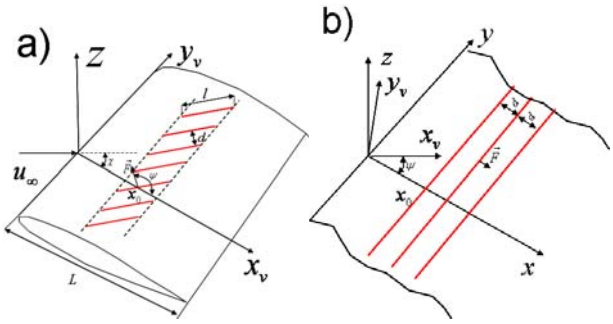

Fig 9. Scheme of multi-electrode actuator for transition control (a) and simplified 2D geometry (b) used for computation of its influence on boundary layer

To delay transition caused by TS waves the electrodes should be parallel to leading edge and ψ should be near zero. Actuator with electrodes normal to leading edge or parallel to external streamlines with $\psi > 90^0$ seems to be most effective for control of cross-flow dominated transition. It is assumed that the action of discharge on the flow can be modeled by the body forces $\vec{F}'$ located in the vicinity of the working edges of each electrode. These forces are assumed to be directed parallel to x axis. Their vertical components can be neglected because of its negligible influence on the flow. Air heating by discharge is rather weak and flow velocity is assumed to be small with respect speed of sound, so model of incompressible fluid with constant density and viscosity will be used further. Non-dimensional variables are introduced using boundary layer thickness $\delta' = (\nu L'/u_\infty)^{1/2}$ and free-stream velocity u_∞ as scales.

The distance between electrodes d is assumed to be small with respect to their length l and l is supposed to be small compared with the chord L. For analysis of the flow near the location of actuator a simplified two-dimensional configuration of infinitely long electrodes shown in Fig. 9, b will be considered. Boundary layer in the vicinity of the actuator is

assumed to be uniform along the electrodes or along the y axis. Profiles of longitudinal (along x axis) U_0 and transversal (along y axis) V_0 in oncoming boundary layer are related with chord-wise U_v and spanwise V_v velocity profiles as

$$U_0 = U_v \cos\psi - V_v \sin\psi$$
$$V_0 = U_v \sin\psi + V_v \cos\psi$$

Solution near the actuator is sought as a sum of this uniform over x,y flow and finite amplitude perturbations of velocity components u,v,w and pressure p induced by discharge. These disturbances are governed by Navier-Stokes equations with the force term $F = F'/\rho u_\infty^2 \delta'$

$$U_0\frac{\partial u}{\partial x} + \frac{dU_0}{dz}w + N_x = -\frac{\partial p}{\partial x} + F + \frac{1}{R}\left(\frac{\partial^2 u}{\partial x^2} + \frac{\partial^2 u}{\partial y^2}\right)$$
$$U_0\frac{\partial v}{\partial x} + \frac{dV_0}{dz}w + N_y = \frac{1}{R}\left(\frac{\partial^2 v}{\partial x^2} + \frac{\partial^2 v}{\partial y^2}\right) \qquad (1)$$
$$U_0\frac{\partial w}{\partial x} + N_z = -\frac{\partial p}{\partial z} + \frac{1}{R}\left(\frac{\partial^2 w}{\partial x^2} + \frac{\partial^2 w}{\partial y^2}\right)$$
$$\frac{\partial u}{\partial x} + \frac{\partial w}{\partial z} = 0$$
$$u,v,w(x,0) = u,v,w(x,\infty) = u,v,w(\pm\infty,z) = 0$$

In these equations $R = u_\infty \delta'/\nu$ is Reynolds number and N_x, N_y, N_z - non-linear terms. Because of perturbations die out at the infinite x they may be presented in form of Fourier integrals

$$\{u,v,w,p\} = \int_{-\infty}^{+\infty}\{u_*,v_*,w_*,p_*\}(k,z)e^{ikx}dk \qquad (2)$$

Application of Fourier transform to (1) and elimination of pressure reduces it to Orr-Sommerfeld and Squire equations

$$U_0(w_*''-k^2w_*) - U_0''w_* = \frac{1}{ikR}(w_*^{IV} - 2k^2w_*'' + k^4w_*) +$$
$$+ F_*' - N_{x*} - ikN_{z*}; \quad w_*(k,0) = w_*'(k,0) = w_*(k,\infty) = 0$$
$$ikU_0v_* = \frac{1}{R}(v_*''-k^2v_*) - N_{y*} \qquad (3)$$
$$v_*(k,0) = v_*(k,\infty) = 0$$

with right parts containing Fourier transforms of body force F_* and non-linear terms N_{x*}, N_{y*}, N_{z*}. Equations (3) were solved for each value of k by matrix method based on collocation technique. Non-linear terms were found by iterations. Solution for perturbations in physical space was found by fast Fourier transform method.

3.2 Phenomenological model of DBD-induced force

Following expression for horizontal component of body force produced by DBD was derived in order to fit available body force distributions computed from PIV data in [8,9] and shown in Fig. 10.

$$F = \theta(\bar{x})\frac{F_\Sigma}{x_0 z_0}\bar{x}\,\bar{z}\,e^{-(\bar{x}+\bar{z})}; \quad \bar{x} = \frac{x}{x_0}; \quad \bar{z} = \frac{z}{z_0} \qquad (4)$$

Here F [N/m^3] – body force density, F_Σ [N/m] – integral force produced by discharge, x_0, z_0 - coordinates of maximum of body force, $\theta(\bar{x})$ - Heaviside function. It includes three constants F_Σ, x_0, z_0 which depend on the parameters of actuator and power supply.

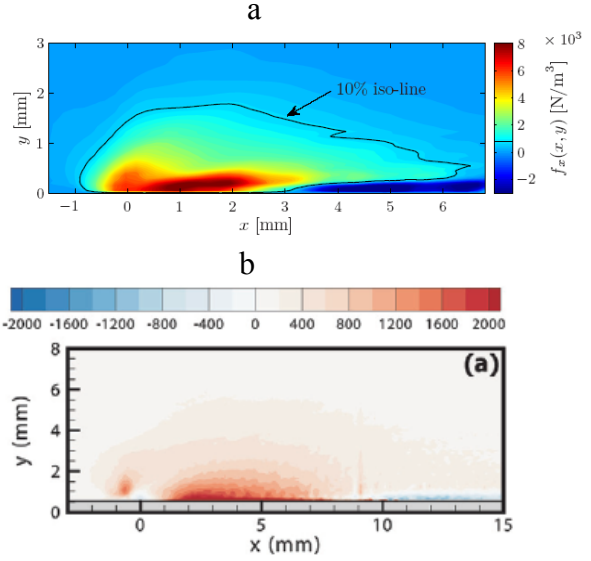

Fig 10. Fields of averaged DBD-induced body force found from PIV data in [8] (a) and [9] (b).

Integral force induced by actuator is usually estimated from its thrust T or impulse of near-wall jet I produced by it. Both of them are smaller than the integral force F_Σ due to

impulse loss to skin friction. To relate the measured values of thrust with integral force F_Σ the propulsive efficiency coefficient η_p is introduced as

$$F_\Sigma = \frac{1}{\eta_t} T \qquad (5)$$

Extensive study of influence of discharge characteristics on the thrust induced by DBD was made in [10]. Results of this work can be approximated by empirical formula

$$T = Af^{0.4}(V - V_0)^2; \quad V_0 = Bf^{-0.2}d^{0.8} \qquad (6)$$

where V[kV] is amplitude of high-voltage, f[kHz] is its frequency and d[mm] is thickness of the dielectric layer, $A = 3.04 \times 10^{-4}$, $B = 2.106$ - empirical constants.

Comparison of thrust found from (6) with experimental data of [10] is presented in Fig. 11. It shows that this formula well approximates all experimental results except of data for actuator with very thin Kapton dielectric.

Coordinates of body force maximum x_0, z_0 can not be measured directly in most of experiments. However, longitudinal extent of the light-emission region L in discharge linearly depends on the amplitude of applied voltage [12]. Assuming the same law for x_0, z_0 dependence from voltage we can write

$$x_0 = C(V - V_0), \quad z_0 = D(V - V_0) \qquad (7)$$

It is naturally to suppose that a threshold voltage V_0 here is the same as in (6). In [12] it is found that length of light-emission region do not depend from frequency. For this reason constants C and D in (7) are assumed to be independent from f. Values of these empirical constants

$$C = 2.8 \times 10^{-4} m/kV; \quad D = 5. \times 10^{-5} m/kV \qquad (8)$$

were chosen in order to fit predicted force distribution with experimental data of [8,9]. Thrust efficiency coefficient in (5) depends both from integral force and vertical coordinate of its maximum. In subsequent computations the value $\eta_t = 0.5$ found from the experimental data for single-electrode actuator operating at regime #1 of generator will be used.

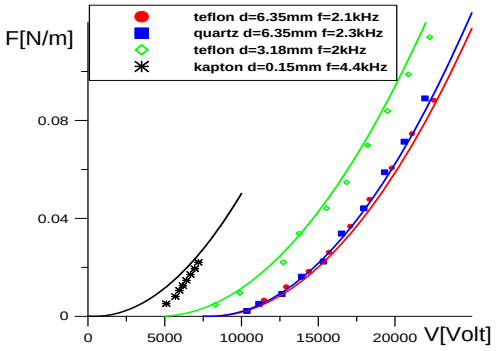

Fig 11. Comparison of empirical correlation for actuator thrust (6) (lines) with experimental data from [10] (points)

Fig. 12 shows body force distributions given by developed model for conditions of experiments [8,9]. This figure demonstrates that the model well describes maximal value of body force and the size of momentum-transfer domain in both experiments.

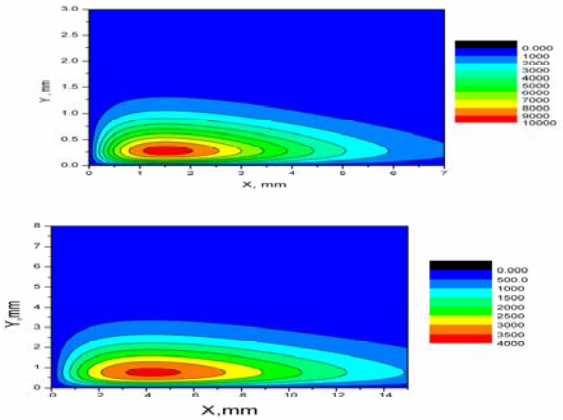

Fig 12. Distribution of body force in of experiments [8] (upper part) and [9] (lower part) found from phenomenological model

To test the model of discharge the flow induced by actuator with one electrode in the still air was computed in the framework of Navier-Stokes equations solution. Distribution of velocity in (x,z) plane are shown in Fig. 13. Maximal velocity takes place at the distance about 2mm behind the edges of electrodes. The velocity field here is similar to this measured by PIV in [11]. Maximal velocity produced by actuator with a single electrode $u_m = 3.5$ m/s

satisfactory coincides with similar value in experiment [11]. Far from actuator the near-wall jet is formed.

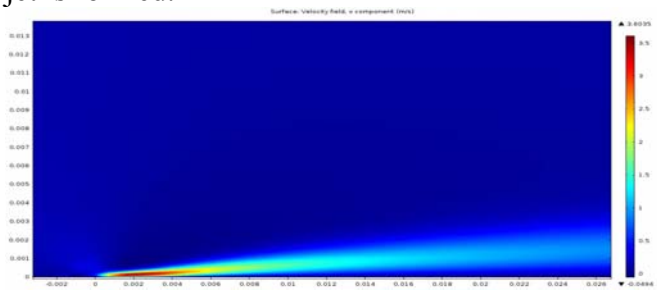

Fig 13. Distributions of streamwise velocity produced by single-electrode actuator in the still air. Computation based on the phenomenological model.

Comparison of velocity profiles in the jet induced by actuator with one electrode at distances 18 and 78mm measured in experiment with similar computational results is presented in Fig. 14. Computed and measured velocities coincide with 10% accuracy.

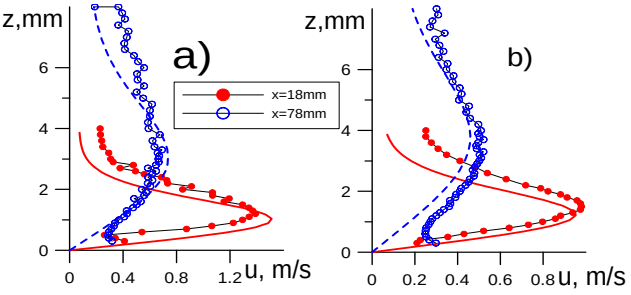

Fig 14. Velocity profiles produced by single-electrode actuator in still air for regimes of generator #1 (a) and #2 (b). Comparison of computation (lines) with experimental data (points).

3.3 Prediction of discharge action on flat-plate boundary layer

Computational method and model of discharge-induced force developed in sections 3.1, 3.2 were used for prediction of boundary layer modification by DBD actuators in conditions of experiment described in section 2. Computations were performed for two types of actuators: single-electrode actuator and three-electrode actuator with distance between electrodes 14mm. Electrodes of all actuators were oriented perpendicular to flow direction ($\psi = 0$) and discharge was initiated by generator operated in regime #1. Discharge induced force used in computations was determined by (4) with $x_0' = 0.67mm$, $z_0' = 0.12mm$ and $F_\Sigma = 7.1\times10^{-3}$ N/m. Computations were performed for flow velocity 10m/s and oncoming Blasius boundary layer for equivalent distance from leading edge 1.4 m. Dimensional boundary layer for this conditions $\delta' = 1.3mm$ and Reynolds number based on it R=920.

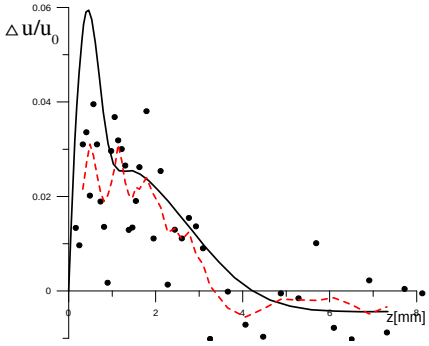

Fig 15. Profiles of increment of streamvise velocity in the boundary layer induced by single-electrode actuator: — - computation, • – experiment, - - - - experiment averaged over 5 points

Comparison of computed profile of increment of streamwise velocity induced by single-electrode actuator at the distance of 18 mm behind the active edge of electrode with experimental data is shown in Fig. 15. Coincidence of the prediction of the model with experiment is rather good in the outer part of the boundary layer. Near the wall the model overestimates flow acceleration induced by discharge. However, velocity increments in this experiment were too small to be accurately measured by hot-wire anemometer.

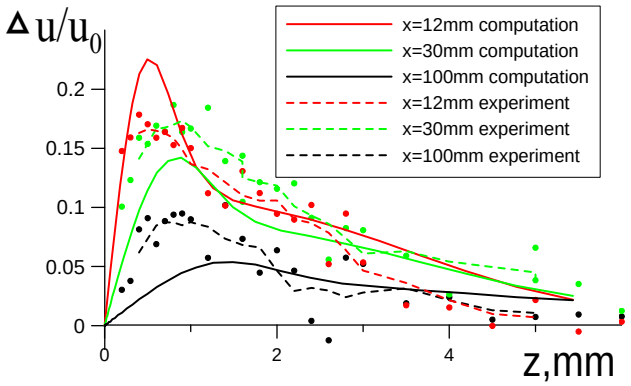

Fig 16. Profiles of increment of streamvise velocity in the boundary layer induced by three-electrode actuator with normal to flow direction electrodes: comparison of computations with experiment

More accurate experimental data were obtained for three-electrode actuator with normal to flow direction electrodes. Measured and computed profiles of velocity increments in this case are plotted in Fig. 16. For this powerful actuator coincidence of computations with experimental data is rather good. This is a promising demonstration of suitability of developed discharge model for prediction of discharge influence on the boundary layer.

3.4 Cross-flow instability control by multi-electrode actuator

Numerical method verified in previous section was applied to numerical modeling of cross-flow instability control by means of multi-electrode actuator. Computations were performed for conditions of planned experiment which will be performed with model of swept-wing section of chord 1m, sweep angle 35^0 and flow velocity 40m/s. Folkner-Scan-Cook self-similar solution

$$U_{0v} = \left(\frac{x'}{L'}\right)^m f'(\eta)\cos\chi; \quad V_{0v} = g'(\eta)\sin\chi$$

$$\eta = \frac{z\sqrt{m\cos\chi}}{\sqrt{\beta}\left(x'/L'\right)^{\frac{1-m}{2}}}; \quad \beta = \frac{2m}{m+1}$$

$$f''' + ff'' + \beta(1 - f'^2) = 0; \quad f(0) = f'(0) = 0; \quad f'(\infty) = 1$$

$$g''' + fg'' = 0; \quad g(0) = g'(0) = 0; \quad g'(\infty) = 1$$

with m=0.29 was used as a model of oncoming boundary layer. It well approximates swept-wing boundary layer in the region of strong cross-flow instability. The actuator was placed at $x' = 0.4\,\text{m}$ and consists from 15 electrodes with period d=14mm inclined with an angle $\psi = 115^0$. For these parameters boundary layer thickness equals to $\delta = 0.6mm$ and Reynolds number based on it was R=1700. Spatial distribution of discharge induced force was the same as in previous section but its amplitude was varied in order to achieve the best elimination of cross-flow in the boundary layer. For this purpose it was expressed as the product of relative amplitude a and integral force value corresponding to regime #1 of generator, that is $F_\Sigma = a \times 7 \times 10^{-3} N/m$. Computations for a=0.5, 0.75 and 1 were performed. Results described below were obtained for simplified 2D geometry of actuator with infinite electrodes shown in Fig. 9,b.

Effect of discharge on the profiles of tangential (along the outer streamlines) and cross-flow velocity profiles in boundary layer shows Fig 17. Here these profiles in oncoming boundary layer together with velocity profiles above the actuator averaged over the distance between 14-th and 15-th electrodes are plotted. Discharge with a=0.75 gives the best elimination of cross-flow. When the amplitude of force is increased to a=1 the discharge initiates positive cross-flow velocity opposite to natural one. Even for optimal amplitude a=0.75 cross flow velocity is not exactly zero, but it is positive near the wall and negative far from it. This is caused by the difference between vertical coordinates of discharge-induced force and cross-flow velocity in oncoming boundary layer. Modification of tangential velocity profile by discharge is rather small.

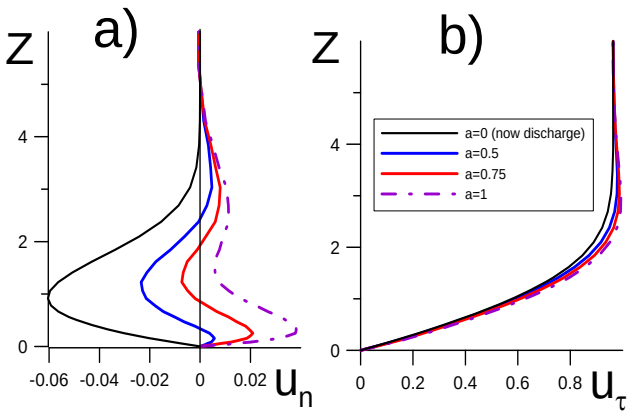

Fig 17. Averaged over the distance between 14th and 15th electrodes profiles of cross-flow (a) and tangential (b) velocity in the boundary layer for different amplitude of discharge-induced force

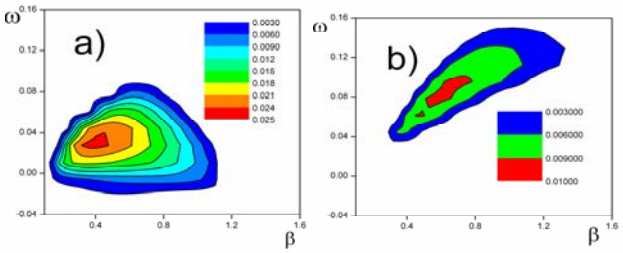

Fig 18. Growth rates of unstable disturbances $\sigma = -\text{Im}(\alpha)$ in oncoming boundary layer (a) and in averaged flow between 14^{th} and 15^{th} electrodes of actuator for a=1 (b).

Influence of discharge with *a=1* on the stability of averaged flow between 14-th and 15-th electrodes shows Fig. 18 where spatial growth rates $\sigma = -\mathrm{Im}(\alpha)$ of unstable modes as function of spanwise wavenumber β and frequency ω are plotted. This figure demonstrates that discharge entirely eliminates instability with respect to steady modes and reduces the maximal growth rate of travelling modes by factor of 3.

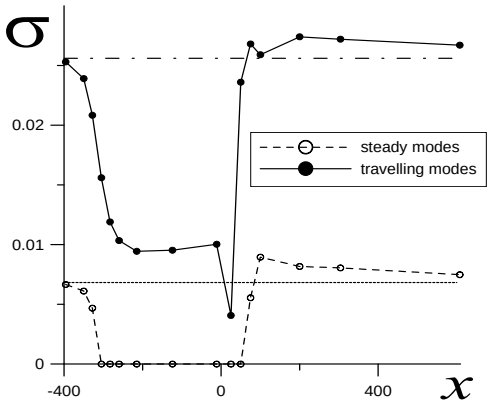

Fig 19. Maximal growth rates of unstable disturbances in the boundary modified by 15-electrode actuator with *a=1*

Next Fig. 19 shows evolution of maximal growth rates of steady and travelling modes along the x –axis (direction normal to electrodes). Almost full stabilizing effect of discharge is reached after the third electrode. After the actuator boundary layer rapidly relaxes to its initial state, so discharge effectively eliminates cross-flow instability only within the actuator area.

Acknowledgments: The work is done in the framework of Buterfli project and under financial support of RFBR grant #13-01-00767

References

[1] Enloe L, McLaughlin T, VanDyken K, Jumper E, Corke T, Post M, et al. Mechanisms and responses of a single dielectric barrier plasma actuator: geometric effects. *AIAA Journal* 2004 v.42, p.585–604

[2] Kotsonis M, Veldhuis L, Bijl H. Plasma assisted aerodynamics for transition delay *Seventh IUTAM Symposium on Laminar-Turbulent Transition*, ed. P. Schlatter, D Henningson, Springer 2010, P.219-224.

[3] Duchmann A., Reeh A., Quadros R., Rriegseis J., Tropea C. Linear stability analysis for manipulated boundary layer flow using plasma actuators. *Seventh IUTAM Symposium on Laminar-Turbulent Transition*, ed. P. Schlatter, D Henningson, Springer 2010, P. 153-158.

[4] Vorobiev A, Rennie R.M., Jumper E. J. Lift enhancement by plasma actuators at low Reynolds numbers *AIAA paper 2010-4836*, 11p.

[5] Kuriachii A.P., Manuilovich S.V. 2009, Suppression of cross-flow induced transition in three-dimensional boundary layer by action of periodic body forces, *in: Models and Methods of Aerodynamics,* Evpatoria 2009„ pp 113-115 (in Russian)

[6] Grundmann S., Tropea C. Delay of boundary layer transition using plasma actuators// *AIAA paper 2008-1369*, 9p.

[7] Hanson R., Lavoie P., Naguib A.M., Morrison J.F. Control of transient growth induced boundary layer transition using plasma actuators. *Seventh IUTAM Symposium on Laminar-Turbulent Transition*, ed. P. Schlatter, D Henningson, Springer 2010, P. 183-188.

[8] Kriegseis J., Shwartz C., Tropea C., Grundmann S. Velocity-information-based force-term estimation of dielectric-barrier discharge plasma actuators. *J. Phys. D: Appl. Phys*. 46 (2013) 055202 (13pp)

[9] Bernard N., Debien A., Moreau E. Time-dependent volume force produced by a non-thermal plasma actuator from experimental velocity field. J. *Phys. D: Appl. Phys.* 46 (2013) 245201 (12pp)

[10] Thomas F.O., Cokke T.C., Iqbal M., Kozlov A., Schatzman D. Optimization of dielectric barrier discharge plasma actuators for active aerodynamics flow control. *AIAA Journal,* 2009, vol.47, p.2169-2178.

[11] . Polivanov P.A., Vishnyakov O.I., Sidorenko A.A., Maslov A.A. Investigation of a nonstationary flow field generated by a dielectric barrier discharge. *Techical Physics*, 2012, vol. 57, № 4, p. 457.

[12] Orlov D., Corke T., Patel M. Electric circuit model for aerodynamic plasma actuator. *AIAA paper №2006-1206.*

Copyright Statement